PAPER

Check for updates

A combined experimental-computational investigation on water adsorption in various ZIFs with the SOD and RHO topologies†

Meizhen Gao, Jing Wang, Zhenghao Rong, Qi Shi [ID]* and Jinxiang Dong [ID]

We synthesized a series of seven zeolitic imidazolate frameworks (ZIFs), namely ZIF-8, ZIF-90, SIM-1, MAF-6, ZIF-25, ZIF-93 and ZIF-97. Then we investigated the adsorption behavior of water for each ZIF *via* a combined experimental-computational method. We focused on the van der Waals (vdW) and electrostatic contributions to their water adsorption capacity. The results showed that the vdW interactions were negligible and that electrostatic interactions played a dominant role. Moreover, we studied the effects of topology in the $[Zn(almeIm)_2]$ system with the same linker, 4-methylimidazole-5-carbaldehyde (almeIm). We found that SIM-1 with a smaller pore size and higher density exhibited greater water adsorption at low relative pressures, and in contrast, ZIF-93 with a larger pore size and lower density had significantly higher adsorption capacity at high relative pressures.

1. Introduction

Zeolitic imidazolate frameworks (ZIFs), as a type of metal–organic framework, are comprised of transition metal ions (Zn, Co, *etc.*) and imidazolate linkers.[1,2] The ZIF structure is connected in a similar manner as zeolites, where the metal ion and imidazolate linker replace the Si/Al and O atoms, respectively. Furthermore, ZIFs are highly stable.[1,2] It is possible to obtain a large number of ZIFs with functional diversity by tuning the various linkers.[1,2] Consequently, the combined properties of ZIFs lead to their potential application for adsorptive separation.[3]

Understanding the water adsorption in ZIFs is valuable for adsorptive separation in industry. For example, hydrophobic ZIFs have been extensively studied for the recovery of organics from dilute aqueous solutions.[4–6] In addition, due to the presence of trace amounts of water in industrial flue gas, the effect of water on CO_2 capture in ZIFs cannot be neglected.[7–9] Therefore, it is indispensable to know the adsorption behavior of water in ZIFs before they are considered as practical adsorbents for industrial purposes.

In recent years, the adsorption of water in ZIFs has been investigated through experiments and simulations. Experimentally, Kaskel *et al.*[10] first reported water vapor adsorption in ZIF-8 and showed that ZIF-8 is a highly hydrophobic material.

Lively *et al.*[11] performed water vapor adsorption in ZIF-71 and found that its water uptake is very small, confirming that this material is hydrophobic. Chance *et al.*[12] studied water vapor adsorption in ZIF-90 and observed that it exhibits hydrophilic properties. Banerjee *et al.*[13] measured the water vapor adsorption and desorption isotherms in CoNIm (RHO), which showed its hydrophilic character. Nair *et al.*[14,15] investigated the water vapor adsorption isotherms of hybrid ZIF-8-90, and they continuously and drastically controlled the hydrophilicity of the ZIFs by tuning the ratio of mixed linkers. Zhang *et al.*[16] reported on the water adsorption in MAF-6. They observed that MAF-6 exhibits high hydrophobicity in both its external crystal surfaces and internal pores. Yang *et al.*[6] recently measured the water vapor adsorption in ZIF-93, ZIF-97, SIM-1, ZIF-90, and ZIF-8. ZIF-8, MAF-6 and ZIF-71 are extremely hydrophobic due to the existence of unfavorable chlorine-based methyl and ethyl groups for water adsorption. The opposite trend in ZIF-90, ZIF-93, SIM-1, CoNIm (RHO) and ZIF-97 was also confirmed, which have hydrophilic carbonyl, nitro and hydroxymethyl groups for water adsorption. To simulate the water adsorption in ZIFs, a few groups applied Monte Carlo (MC) techniques. Nieto-Draghi *et al.*[17] evaluated the hydrophobicity and hydrophilicity of ZIFs using the ideal adsorption heat and Henry's constant. Coudert *et al.*[18] demonstrated how linker functionalization, geometry and topology drastically influence the water adsorption *via* GCMC simulation on a series of ZIFs. Jiang *et al.*[19,20] simulated water adsorption in a series of ZIFs. Simulation results showed that ZIFs with functional groups that can form H-bonds and can be regarded as hydrophilic; whereas, the ZIFs that have functional groups with no H-bonding formed can be classified as hydrophobic. Thus, the adsorption mechanism of

Research Institute of Special Chemicals, College of Chemistry and Chemical Engineering, Taiyuan University of Technology, Taiyuan 030024, China. E-mail: shiqi594@163.com

water is ascribed to the interactions that enhance H-bonds formation between water and the polar groups of ZIFs.

According to the experimental and computational studies mentioned above, water adsorption is sensitive to the functional groups of ZIFs. However, the role of vdW and electrostatic interactions between water and ZIFs has not been investigated to date. In this work, various ZIFs based on the SOD and RHO topology were studied systematically using a combined experimental-computational investigation to examine the impact of the functional groups of ZIFs on their water adsorption properties. We analyzed each contribution of the electrostatic and vdW interactions to the water adsorption capacity to reveal the adsorption behavior of water in ZIFs. Finally, we studied the effect of topology in the $[Zn(almeIm)_2]$ system with the same linker, 4-methylimidazole-5-carbaldehyde (almeIm).

2. Computational details

2.1 ZIF structures

In this study, we measured water adsorption in seven ZIFs. Fig. 1a and b show the structures of one cage and imidazolate linkers of the ZIFs, respectively. Specifically, among the seven ZIFs, there were two types of topologies, SOD and RHO. The SOD-type topology was connected by 4- and 6-membered rings and the RHO type was connected by 4-, 6-, and 8-membered rings. The SOD topology included ZIF-8, ZIF-90, and SIM-1. The linkers of ZIF-8 and ZIF-90, 2-methylimidazole (mIm) and imidazole-2-carboxaldehyde (Ica), were singly functionalized on position 2; while, the linker of SIM-1, 4-methylimidazole-5-carbaldehyde (almeIm), was dually functionalized at the 4 and 5 positions. The RHO topology contained MAF-6, ZIF-25, ZIF-93, and ZIF-97. The linker of MAF-6, 2-ethylimidazole (eIm), was singly functionalized on position 2; while, the linkers of ZIF-25, ZIF-93, and ZIF-97, 4,5-dimethyl-1*H*-imidazole (dmeIm), 4-methylimidazole-5-carbaldehyde (almeIm), and 4-hydroxymethyl-5-methylimidazole (hymIm), respectively, were dual-functionalized at the 4 and 5 positions.

The crystal structures of all the ZIFs except for ZIF-25 were obtained from the published literature. The structure of ZIF-8,[1] ZIF-90,[21] ZIF-93,[22] and ZIF-97 (ref. 22) was constructed by Yaghi *et al.*, SIM-1 (ref. 23) was built by combining experimental and computational methods and MAF-6 (ref. 24) was published by Chen *et al.* For ZIF-25, we manually constructed its initial structure based on a single crystal of ZIF-71 (ref. 25) using Materials Studio Visualizer. Table 1 summarizes the structural parameters of the studied ZIFs. Our simulations used crystal structures that were optimized with the Forcite module in the geometry optimization algorithm.

2.2 Force field

The interaction of adsorbate–adsorbent and adsorbate–adsorbate was described by a combination of Lennard-Jones (LJ) and coulombic potentials:

$$U_{\text{nonbended}} = \sum \left\{ 4\varepsilon_{ij} \left[\left(\frac{\sigma_{ij}}{\gamma_{ij}} \right)^{12} - \left(\frac{\sigma_{ij}}{\gamma_{ij}} \right)^{6} \right] + \left(\frac{q_i q_j}{4\pi\varepsilon_0 \gamma_{ij}} \right) \right\}$$
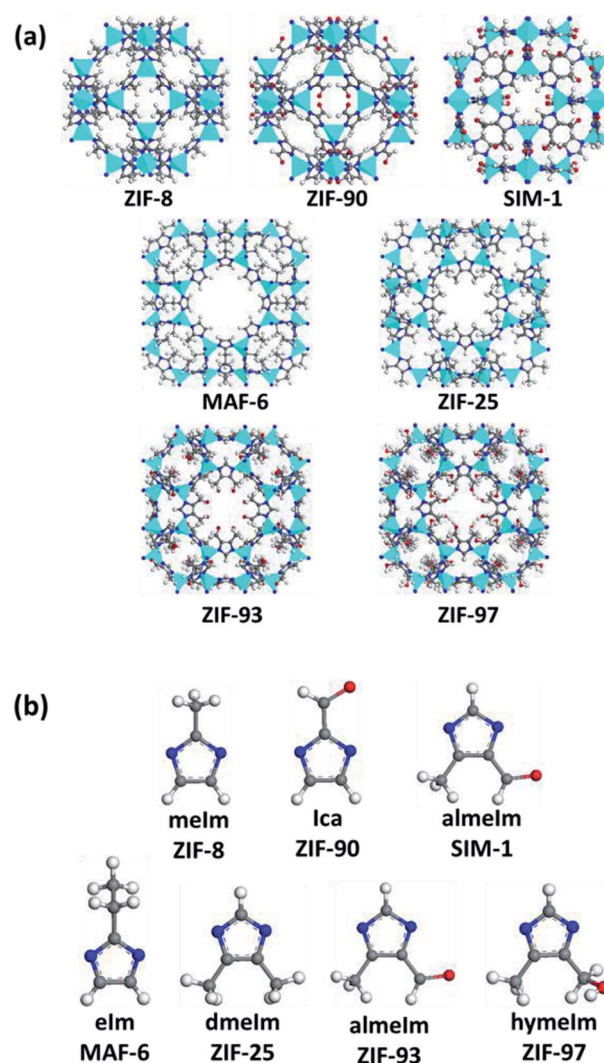

Fig. 1 (a) Structures of one cage of ZIF-8, ZIF-90, SIM-1, MAF-6, ZIF-25, ZIF-93, and ZIF-97 and (b) imidazolate linkers of the corresponding ZIFs. Atom colors: zinc, cyan tetrahedral; C: gray; N: dark blue; O: red; and H: white.

where, σ_{ij} and ε_{ij} are the collision diameter and the well depth, respectively, q_i refers to the charge of atom i, γ_{ij} represents the distance between atoms i and j, and the permittivity of vacuum $\varepsilon_0 = 8.8542 \times 10^{-12} \text{ C}^2 \text{ N}^{-1} \text{ m}^{-2}$. The partial atomic charges in the ZIFs were calculated *via* the density functional theory (DFT) on fragmental clusters (see Fig. S1–S7, ESI†). The DFT calculations were performed with the Gaussian 09 software using the B3LYP functional combined with the LanL2DZ basis set for the Zn atom and the 6-31G (d) basis set for all other atoms. The partial atomic charges were estimated by fitting the electrostatic potentials (see Tables S1–S7, ESI†). The DREIDING force field was successfully used by Jiang *et al.*[19] to describe the water adsorption in ZIFs. Therefore, we also used the DREIDING in this work. The LJ potential parameters of the ZIFs are listed in Table S8 (ESI).†

The water molecules were described as a rigid three-point transferable interaction potential (TIP3P) model.[26] It has been

Table 1 Structural parameters of the seven ZIFs

ZIF	ZIF-8	ZIF-90	SIM-1	MAF-6	ZIF-25	ZIF-93	ZIF-97
Topology	SOD	SOD	SOD	RHO	RHO	RHO	RHO
Linker	meIm	Ica	almeIm	eIm	dmeIm	almeIm	hymeIm
Space group	$I\bar{4}3m$	$I\bar{4}3m$	$I23$	$Im\bar{3}m$	$Pm\bar{3}m$	$I432$	$I432$
Unit cell (Å)	16.9910	17.2715	33.4870	29.2582	28.5539	28.3565	28.4319
ρ^a (g cm^{-3})	0.924	0.988	1.204	0.814	0.875	0.991	0.997
S^b (m^2 g^{-1})	1643	1150	602	1402	1304	882	854
V^c (cm^3 g^{-1})	0.66	0.57	0.29	0.62	0.54	0.42	0.36

^{a} Computational densities of perfect crystals. ^{b} Experimental BET surface areas. ^{c} Experimental pore volume.

demonstrated that the TIP3P model shows a good interaction potential when compared with experimental measurements.[27] Table S9 (ESI†) lists all the TIP3P parameters of water. The LJ cross potential parameters were determined using the Lorentz–Berthelot mixing rules.

2.3 Adsorption simulations

The grand-canonical Monte Carlo (GCMC) method was applied to simulate water adsorption in the studied ZIFs. The adsorption was performed below the saturation vapor pressure of water; thus, water was treated as an ideal gas. The saturation vapor pressure of water is $P_0 = 3.14$ kPa at 298 K in ref. 19. All adsorption processes were simulated at 298 K. It has been shown that framework flexibility has almost no influence on gas adsorption in ZIFs;[28] hence, the ZIFs were regarded as rigid during simulations. The simulation box contained eight ($2 \times 2 \times 2$) unit cells for ZIF-8 and ZIF-90 and one unit cells for SIM-1, MAF-6, ZIF-25, ZIF-93, and ZIF-97. Periodic boundary conditions were employed in all three dimensions. The cutoff radius of 12.8 Å was set for the LJ interactions, and the Ewald sum method was applied to handle the long-range electrostatic interactions. All GCMC simulations included 1.0×10^7 steps to reach equilibration, followed by 1.0×10^7 steps to sample the desired thermodynamic properties. The GCMC simulations were conducted using the sorption code in Materials Studios 8.0.[29]

To evaluate adsorption energy, the single-molecule MC method was performed to simulate the heat of adsorption at infinite dilution, Q_{st}^0. The heat of adsorption, Q_{st}^0, was calculated as follows:[19]

$$Q_{st}^0 = R_g T - U_{ad}^0$$

$$U_{ad}^0 = U_{total} - (U_{adsorbent} + U_{adsorbate})$$

where, T is temperature, R_g is the gas constant, $U_{adsorbate}$, $U_{adsorbent}$ and U_{total} are the potential energies of the a single adsorbate molecule, adsorbent and adsorbent–adsorbate, respectively.

3. Experimental section

3.1 ZIF synthesis

3.1.1 ZIF-8. ZIF-8 was synthesized by modifying the method proposed by Yaghi et al.[1] Zinc acetate dihydrate (0.220 g, 1

mmol) and 2-methylimidazole (0.246 g, 3 mmol) were dissolved in MeOH (15 mL) in a 30 mL Teflon-lined autoclave. The sealed autoclave was heated in an oven at 100 °C for 3 days. The sample was collected and activated by soaking in MeOH and then drying under vacuum for 12 h at 150 °C.

3.1.2 ZIF-90. ZIF-90 was synthesized by modifying the method proposed by Yaghi et al.[21] A solution of zinc acetate dihydrate (0.220 g, 1 mmol) in MeOH (8 mL) and a solution of imidazole-2-carboxaldehyde (0.360 g, 4 mmol) in MeOH (8 mL) were combined in a 30 mL Teflon-lined autoclave, which was heated in an oven at 50 °C for 1 day. The sample was collected and activated by soaking in MeOH and then drying under vacuum for 12 h at 150 °C.

3.1.3 SIM-1. SIM-1 was synthesized by modifying the approach published by Aguado et al.[30] Zinc acetate dihydrate (0.220 g, 1 mmol) and 4-methylimidazole-5-carbaldehyde (0.165 g, 1.5 mmol) were dissolved in DMF (15 mL) in a 30 mL Teflon-lined autoclave. Then the sealed autoclave was heated in an oven at 100 °C for 1 day. The sample was collected and activated by soaking in MeOH and then drying under vacuum for 12 h at 150 °C.

3.1.4 MAF-6. MAF-6 was synthesized as reported by Zhang et al.[16] A concentrated aqueous ammonia solution (25–28%, 30 mL) of Zn(OH)$_2$ (0.199 g, 2 mmol) was added to a methanol solution (30 mL) of 2-ethylimidazole (0.288 g, 3 mmol) premixed with cyclohexane (3 mL). The resultant slurry was stirred at room temperature for 0.5 h. The sample was collected and activated by soaking in MeOH and then drying under vacuum for 12 h at 150 °C.

3.1.5 ZIF-25. ZIF-25 was synthesized according to the procedure published by Yaghi et al.[22] Zinc acetate dihydrate (0.220 g, 1 mmol) and 4,5-dimethyl-1H-imidazole formate (0.427 g, 3 mmol) were dissolved in MeOH (15 mL) in a 30 mL Teflon-lined autoclave. The sealed autoclave was heated in an oven at 120 °C for 1 day. The sample was collected and activated by soaking in MeOH and then drying under vacuum for 12 h at 85 °C.

3.1.6 ZIF-93. ZIF-93 was synthesized according to the procedure published by Yaghi et al.[22] Zinc acetate dihydrate (0.220 g, 1 mmol) and 4-methylimidazole-5-carbaldehyde (0.330 g, 3 mmol) were dissolved in MeOH (15 mL) in a 30 mL Teflon-lined autoclave. The sealed autoclave was heated in an oven at 85 °C for 1 day. The sample was collected and activated by soaking in MeOH and then drying under vacuum for 12 h at 85 °C.
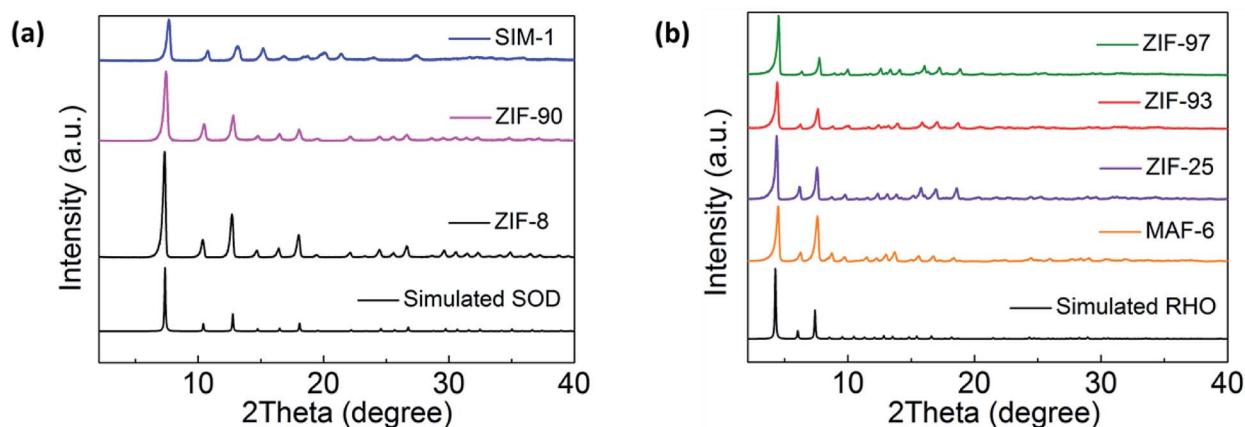
Fig. 2 (a) PXRD patterns of ZIF-8, ZIF-90, and SIM-1 compared with the simulated SOD pattern. (b) PXRD patterns of MAF-6, ZIF-25, ZIF-93, and ZIF-97 compared with the simulated RHO pattern.

3.1.7 ZIF-97. ZIF-97 was synthesized according to the procedure published by Yaghi *et al.*[22] Zinc acetate dihydrate (0.220 g, 1 mmol) and 4-hydroxymethyl-5-methylimidazole (0.560 g, 5 mmol) were dissolved in DMF (15 mL) in a 30 mL Teflon-lined autoclave. The sealed autoclave was heated in an oven at 100 °C for 1 day. The sample was collected and activated by soaking in MeOH and then drying under vacuum for 12 h at 85 °C.

3.2 Characterization

The ZIF samples were characterized *via* powder X-ray diffraction (PXRD), thermal gravimetry (TG), N_2 adsorption, and scanning electron microscopy (SEM). PXRD data was obtained on an X-ray diffractometer (Rigaku, MiniFlex II) with Cu Kα radiation ($\lambda = 1.5418$ Å). TG analysis was conducted at a heating rate of 5 °C min^{-1} under an air atmosphere using a simultaneous thermal analyzer (Labsystems Evo, Setaram). Surface area and pore volume were assessed by measuring the N_2 adsorption isotherms at 77 K on an automated volumetric adsorption apparatus (Micromeritics, ASAP2020). SEM images were obtained with a scanning electron microscope (Hitachi, SU8010).

3.3 Adsorption isotherm measurement

The water vapor adsorption isotherms at 298 K were measured on an automated gravimetric sorption analyzer (Surface Measurement Systems, DVS Intrinsic). The activated samples were mounted on a balance, and the water sorption was analyzed at relative pressure P/P_0 (P_0 is the saturation vapor pressure) ranging from 0–0.9 ($P/P_0 = 0$, 0.1, 0.2, 0.3, 0.4, 0.5, 0.6, 0.7, 0.8 and 0.9) until the sample reached equilibrium. Equilibrium was considered to be achieved if less than 0.002% weight change was observed in 10 min and the maximum time limit for each step was 360 min.

4. Results and discussion

4.1 Material characterization

To confirm the bulk purity of all the samples, PXRD data was recorded for all the ZIFs. The experimental PXRD patterns of ZIF-8, ZIF-90 and SIM-1 were compared with the simulated powder pattern of ZIF-8, which had the same SOD topology (Fig. 2a). The experimental PXRD patterns of MAF-6, ZIF-25, ZIF-93, and ZIF-97 were compared with the simulated powder
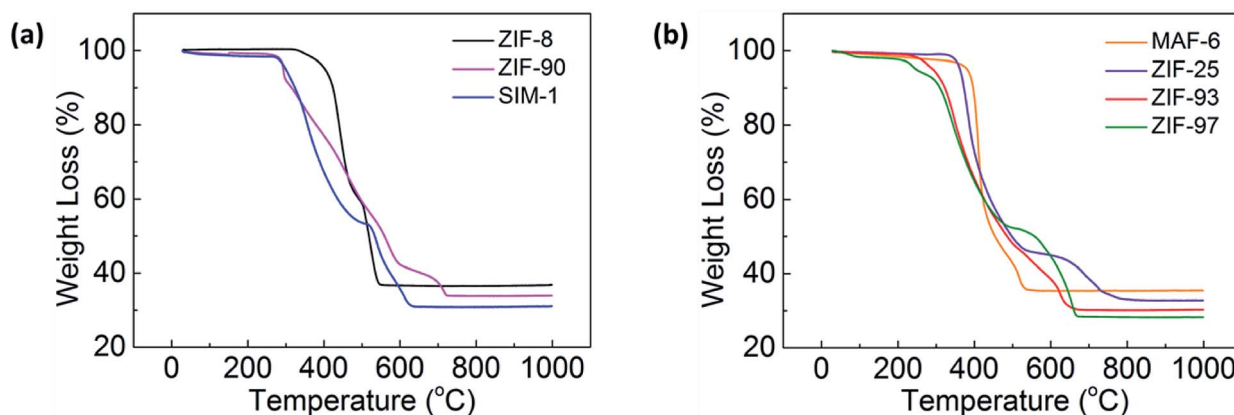

Fig. 3 TG curves of (a) ZIF-8, ZIF-90, and SIM-1 and (b) MAF-6, ZIF-25, ZIF-93, and ZIF-97.

pattern of MAF-6, which had the same RHO topology (Fig. 2b). The results demonstrated that these ZIF materials were pure.

In addition, TG was performed to confirm that guest molecules were removed from the pores of the ZIFs. Fig. 3a and b present the TG curves of the SOD-type ZIFs and RHO-type ZIFs, respectively. The TG curves of all the activated samples exhibited no loss in sample mass from RT to 200 °C, which meant that the guest molecules in the pores were removed. All the ZIFs were finally broken down into ZnO, and the experimental values (36.5, 33.8, 30.9, 35.3, 32.7, 30.2, and 28.2 wt% for ZIF-8, ZIF-90, SIM-1, MAF-6, ZIF-25, ZIF-93, and ZIF-97) were in good agreement with the corresponding calculated values (35.8, 31.9, 28.7, 31.8, 31.8, 28.7, and 28.3 wt%), respectively.

To further characterize the ZIF materials, N_2 adsorption studies were also conducted. Fig. 4a and b show the N_2 adsorption/desorption isotherms of the SOD-type ZIFs and RHO-type ZIFs, respectively. The type I isotherms observed for all the ZIFs revealed their microporous properties. In addition, the N_2 adsorption isotherm of ZIF-90 showed a step at about $P/P_0 = 0.3$, which is in agreement with the results of the SEM

analysis and proves the existence of mesopores between the primary nanoparticles formed a porous feature in the external surface (Fig. S8, ESI†). The BET surface areas were calculated to be 1643, 1150, 602, 1402, 1304, 882, and 854 m^2 g^{-1} for ZIF-8, ZIF-90, SIM-1, MAF-6, ZIF-25, ZIF-93, and ZIF-97, with a pore volume of 0.66, 0.57, 0.29, 0.62, 0.54, 0.42, and 0.36 cm^3 g^{-1}, respectively.

To examine the morphology of the ZIF samples, Fig. 5 shows their representative SEM images. As can be seen from the SEM images, the morphology of the ZIFs was polyhedral. The typical particle size was about 10 μm for ZIF-8, and the relatively uniform average particle sizes were approximately 20 μm, 3 μm, 500 nm, 10 μm, and 3 μm for ZIF-90, SIM-1, MAF-6, ZIF-25, and ZIF-97, respectively. For ZIF-93, its morphology was non-uniform aggregates and its typical particle size was 0.5 μm.

4.2 Water vapor adsorption

4.2.1 Analysis of hydrophobic and hydrophilic ZIFs. To study the hydrophobicity or hydrophilicity of the ZIFs, their adsorption isotherms and heats of adsorption of water were
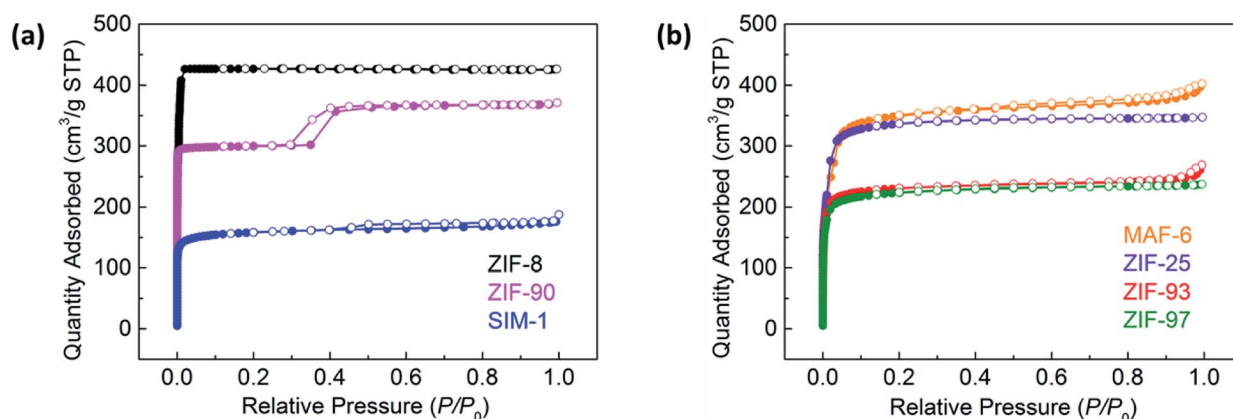

Fig. 4 N_2 adsorption/desorption isotherms at 77 K of (a) ZIF-8 (black), ZIF-90 (magenta), and SIM-1 (blue) and (b) MAF-6 (orange), ZIF-25 (purple), ZIF-93 (red), and ZIF-97 (green). The filled and empty symbols denote the adsorption and desorption isotherms, respectively.
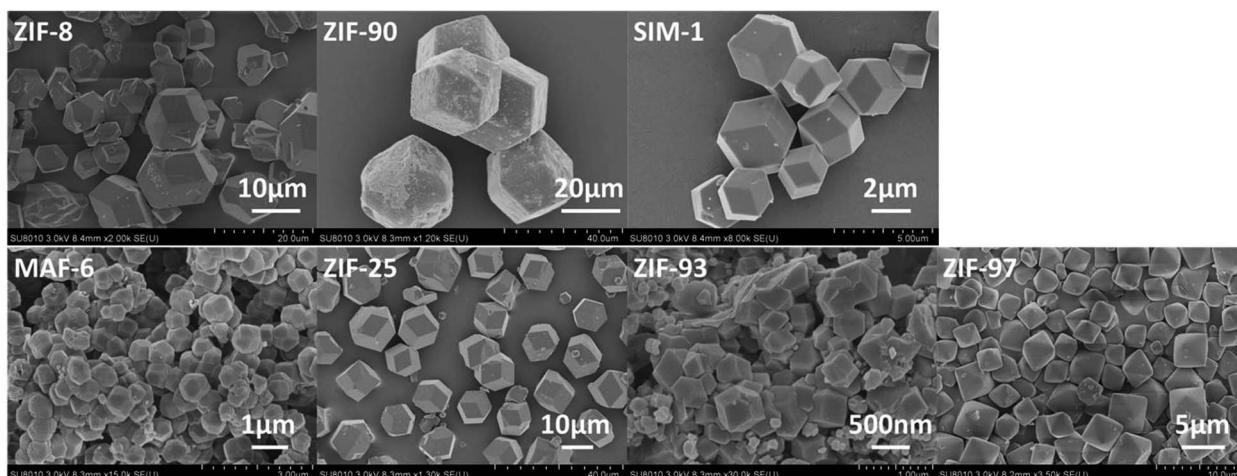

Fig. 5 SEM images of the ZIF-8, ZIF-90, SIM-1, MAF-6, ZIF-25, ZIF-93, and ZIF-97 samples.

obtained. First, we compared the simulated and experimental water adsorption isotherms at 298 K for each ZIF to verify the feasibility of the simulation, as shown in Fig. 6a and b. The filled and empty symbols represent the simulated results and experimental data, respectively. The water uptake in ZIF-8, MAF-6, and ZIF-25 was very low, as observed from both simulation and experimentation. For ZIF-90, the water uptake was initially low, but sharply increased beyond the relative pressure of $P/P_0 = 0.3$. In the low relative pressure region, fairly good agreement was observed between the simulated and experimental data, and similarly, in the high-relative pressure region, the simulation gave acceptable agreement with the experimental results. For ZIF-93, similar to that of ZIF-90, water uptake slowly increased at a low relative pressure but sharply increased beyond $P/P_0 = 0.4$. In the low relative pressure region, the deviation between the simulated and experimental data was larger due to the certain distortion in the structural formula of the partial 4-methylimidazole-5-carbaldehyde on ZIF-93 used in the simulation (see Fig. S6,† where the imidazole ring and aldehyde group are not in the same plane). In the high relative pressure region, the simulation showed reasonable agreement with the experimental data. For SIM-1 and ZIF-97, the water uptake gradually increased at low relative pressures and then slowly increased. The simulations showed relatively good

agreement with the experimental results, although they overestimated at low relative pressures and underestimated at high relative pressures. These acceptable deviations between the simulation and experiment may be because the experimentally synthesized crystals were not perfect and some of the crystal structures were not experimentally solved. Overall, with the notable exception of water adsorption in ZIF-93 at low relative pressures, although there was certain deviation between the simulation and experimental results, these deviations were within the normal, expected range. Therefore, we contend that the computer model was feasible, and thus, it was further used to simulate the adsorption heats at infinite dilution of each ZIF.

Adsorption heat is one of the important indicators used to measure the adsorption capacity of adsorbents. Here, the heat of adsorption at infinite dilution, Q_{st}^0, reflected the interaction between a single water molecule and the individual ZIF. Fig. 7 shows the simulated heats of water adsorption in ZIF-8, ZIF-90, SIM-1, MAF-6, ZIF-25, ZIF-93, and ZIF-97. Among the seven ZIFs, SIM-1, ZIF-93, ZIF-97, and ZIF-90 exhibited higher Q_{st}^0 (more than 30 kJ mol^{-1}) than ZIF-8, MAF-6, and ZIF-25 due to their polar –CHO and –CH$_2$OH groups. With polar functional groups, SIM-1, ZIF-93, ZIF-97, and ZIF-90 formed H-bonds with H$_2$O and promoted H$_2$O adsorption. In contrast, the non-polar groups (–CH$_3$ and –C$_2$H$_5$) in ZIF-8, MAF-6, and ZIF-25 did not form H-bonds with H$_2$O, and the H$_2$O-ZIF interactions were very weak. In addition, the order of Q_{st}^0, ZIF-93 > ZIF-97 > ZIF-90 > ZIF-8, is consistent with the study by Nieto-Draghi et al.[17] The specific values of water adsorption heat from our simulation and reported simulation are available in Table S10 (ESI†).

In this study, we determined the hydrophilic or hydrophobic property of the ZIFs via the combination of water uptake and the heat of adsorption, Q_{st}^0. From the discussion above, we contend that ZIF-8, MAF-6, and ZIF-25 can be treated as hydrophobic because their water uptake was negligible and Q_{st}^0 was small, which was substantially lower than the heat of vaporization of water (45.85 kJ mol^{-1}); whereas, SIM-1, ZIF-93, ZIF-97, and ZIF-90 can be regarded as hydrophilic because their water uptake was substantial and Q_{st}^0 was large.
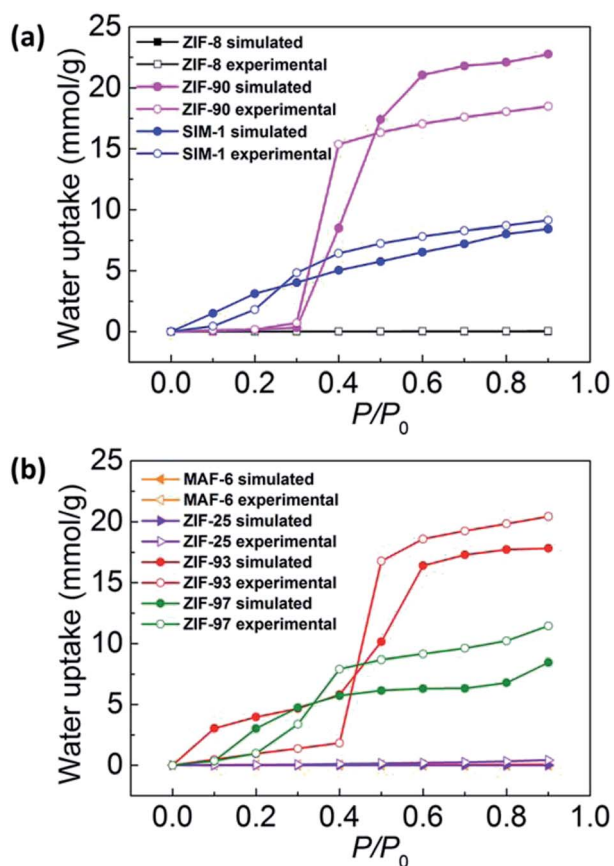

Fig. 6 Simulated (filled symbols) and experimental (empty symbols) water adsorption isotherms at 298 K of (a) ZIF-8 (black), ZIF-90 (magenta), and SIM-1 (blue) and (b) MAF-6 (orange), ZIF-25 (purple), ZIF-93 (red), and ZIF-97 (green).
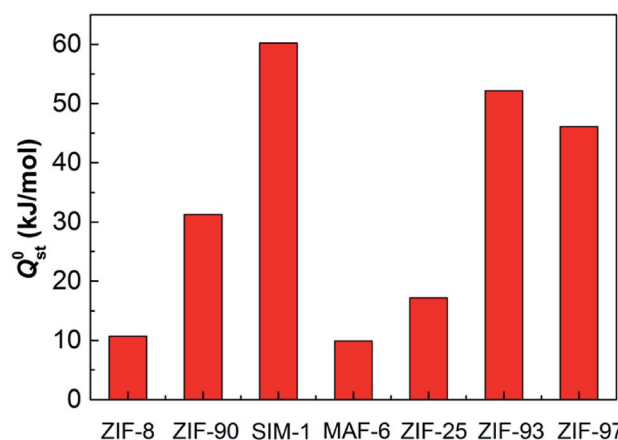

Fig. 7 Simulated adsorption heats at infinite dilution for water adsorption in ZIF-8, ZIF-90, SIM-1, MAF-6, ZIF-25, ZIF-93, and ZIF-97.
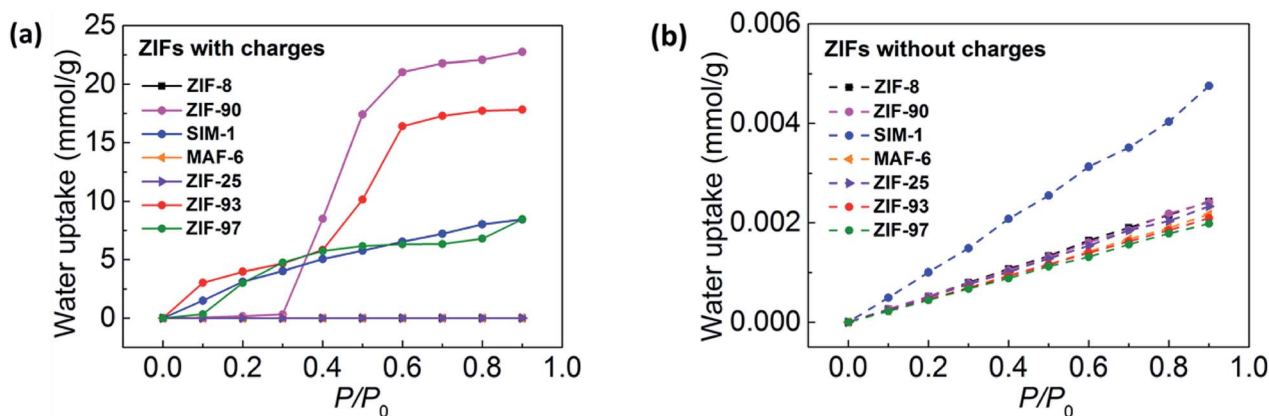
Fig. 8 Simulated water adsorption isotherms at 298 K for each ZIF (a) with atomic charges (solid lines) and (b) without atomic charges (dashed lines).

4.2.2 Role of the vdW and electrostatic interactions. The adsorption uptake was the result of the joint contribution of the vdW and electrostatic interactions. To reveal the role of each contribution, we simulated the water adsorption isotherms at 298 K of each ZIF with and without charges. When the simulation was conducted with atomic charges in the ZIFs, the model simulated both the short-range vdW interactions and long-range electrostatic interactions, as shown in Fig. 8a. When the simulation was performed without atomic charges in the ZIFs, the model only simulated the short-range vdW interactions modeled by DREIDING potentials, as shown in Fig. 8b. Here, we defined the contributions of the vdW interactions and electrostatic interactions as N_{vdW} and $N_{total} - N_{vdW}$, respectively, where N_{vdW} and N_{total} represent the water uptake without and with atomic charges in the ZIFs, respectively.

First, we analyzed the role of the vdW interactions. As can be seen in Fig. 8b, the water adsorption in the different ZIFs showed almost no difference and the water uptake N_{vdW} was nearly zero. This demonstrates that the contribution of the vdW interaction is negligible for water adsorption in ZIFs.

Next, we illustrated the role of the electrostatic interactions. We found that the magnitude of contribution of the electrostatic interactions was related to the functional groups. As shown in Fig. 8a and b, for the hydrophobic ZIF-8, MAF-6, and ZIF-25 with non-polar groups, the water uptake was nearly zero for both N_{total} and N_{vdW}; that is, $N_{total} - N_{vdW}$ was nearly zero. Whereas, for the hydrophilic SIM-1, ZIF-93, ZIF-97, and ZIF-90 with polar groups, N_{total} was large but N_{vdW} was nearly zero, that is, $N_{total} - N_{vdW}$ was large. Thus, this shows that the electrostatic interactions play a dominant role in enhancing water adsorption in ZIFs. This is due to the high polarity of the water molecule. In addition, we discovered that the electrostatic interactions were strongly affected by the functional group polarity. In conclusion, the data shows that the polarity of the functional groups of the ZIF framework is the main factor determining its hydrophobicity or hydrophilicity.

Furthermore, we also simulated the CO_2 adsorption in ZIF-25 and ZIF-93 (Fig. S9, ESI†). We discovered that the high CO_2 adsorption is ascribed to the joint contribution of the vdW and

electrostatic interaction. This phenomenon is different from water adsorption.

4.2.3 Effect of topology: SIM-1 (SOD) and ZIF-93 (RHO). To study the effect of topology on water adsorption in ZIFs, we assessed SIM-1 (SOD) and ZIF-93 (RHO) with the same imidazolate linkers and metal ions. Since there was a certain deviation between the simulations and experimental results on water adsorption in ZIF-93 at low relative pressures, we selected the experimentally measured water adsorption isotherms of SIM-1 and ZIF-93 for comparison, as shown in Fig. 9. At low relative pressures, SIM-1 with smaller pores and higher density had a greater adsorption of water than ZIF-93 with larger pores and lower density. In contrast, at high relative pressures, ZIF-93 had significantly higher adsorption than SIM-1. This phenomenon was also been observed by Laird et al.[31] for CO_2 adsorption in ZIFs. This implied that topological changes have a significant impact on adsorption. In addition, we also studied the effect of particle size on water adsorption and the experimental results showed that particle size of ZIFs has little effect on adsorption (Fig. S11, ESI†).
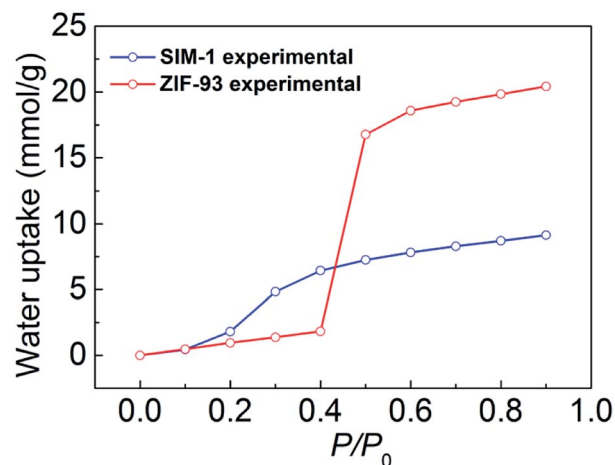

Fig. 9 Experimental water adsorption isotherms at 298 K of SIM-1 and ZIF-93.

5. Conclusions

In this study, we synthesized seven ZIFs with different topologies and imidazolate linkers and studied their water vapor adsorption *via* a combination of experimental measurements and computational simulations. We described the hydrophobicity or hydrophilicity of ZIFs using both their adsorption isotherms and adsorption heats. With non-polar groups, ZIF-8, MAF-6, and ZIF-25 did not form H-bonds with H_2O and had weak interactions with H_2O, which gave rise to a very small water uptake and Q_{st}^0, and thus, they are highly hydrophobic. With polar groups, SIM-1, ZIF-93, ZIF-97, and ZIF-90 formed H-bonds with H_2O and promoted H_2O adsorption, which resulted in a larger water uptake and Q_{st}^0, and thus they can be considered hydrophilic.

In addition, we focused on analyzing the role of the vdW and electrostatic interactions in water adsorption of ZIFs. Our results demonstrated that the contribution of vdW interactions is negligible and the contribution of electrostatic interactions plays a dominant role. The electrostatic interactions between water and the ZIFs were strongly affected by their functional group polarity. Finally, we compared the water adsorption of SIM-1 (SOD) and ZIF-93 (RHO) to investigate the effects of topology. The experimental results showed that SIM-1 with a smaller pore size and higher density had a greater water adsorption at low relative pressures, and in contrast, ZIF-93 with a larger pore size and lower density had significantly higher adsorption at high relative pressures.

Conflicts of interest

There are no conflicts to declare.

Acknowledgements

Notes and references

1 K. S. Park, Z. Ni, A. P. Cote, J. Y. Choi, R. Huang, F. J. Uribe-Romo, H. K. Chae, M. O'Keeffe and O. M. Yaghi, *Proc. Natl. Acad. Sci. U. S. A.*, 2006, **103**, 10186–10191.

2 A. Phan, C. J. Doonan, F. J. Uriberomo, C. B. Knobler, M. O'Keeffe and O. M. Yaghi, *Acc. Chem. Res.*, 2010, **43**, 58–67.

3 B. R. Pimentel, A. Parulkar, E. K. Zhou, N. A. Brunelli and R. P. Lively, *ChemSusChem*, 2014, **7**, 3202–3240.

4 C. Gao, Q. Shi and J. Dong, *CrystEngComm*, 2016, **18**, 3842–3849.

5 H. Jin, Y. Li, X. Liu, Y. Ban, Y. Peng, W. Jiao and W. Yang, *Chem. Eng. Sci.*, 2015, **124**, 170–178.

6 H. Jin, Y. Li and W. Yang, *Ind. Eng. Chem. Res.*, 2018, **57**, 11963–11969.

7 H. Huang, W. Zhang, D. Liu and C. Zhong, *Ind. Eng. Chem. Res.*, 2012, **51**, 10031–10038.

8 Y. Liu, J. Liu, Y. S. Lin and M. Chang, *J. Phys. Chem. C*, 2014, **118**, 6744–6751.

9 J. Hu, Y. Liu, J. Liu and C. Gu, *Fuel*, 2017, **200**, 244–251.

10 P. Küsgens, M. Rose, I. Senkovska, H. Fröde, A. Henschel, S. Siegle and S. Kaskel, *Microporous Mesoporous Mater.*, 2009, **120**, 325–330.

11 R. P. Lively, M. E. Dose, J. A. Thompson, B. A. McCool, R. R. Chance and W. J. Koros, *Chem. Commun.*, 2011, **47**, 8667–8669.

12 K. Zhang, R. P. Lively, M. E. Dose, A. J. Brown, C. Zhang, J. Chung, S. Nair, W. J. Koros and R. R. Chance, *Chem. Commun.*, 2013, **49**, 3245–3247.

13 B. P. Biswal, T. Panda and R. Banerjee, *Chem. Commun.*, 2012, **48**, 11868–11870.

14 K. Eum, K. C. Jayachandrababu, F. Rashidi, K. Zhang, J. Leisen, S. Graham, R. P. Lively, R. R. Chance, D. S. Sholl and C. W. Jones, *J. Am. Chem. Soc.*, 2015, **137**, 4191–4197.

15 K. C. Jayachandrababu, D. S. Sholl and S. Nair, *J. Am. Chem. Soc.*, 2017, **139**, 5906–5915.

16 C. T. He, L. Jiang, Z. M. Ye, R. Krishna, Z. S. Zhong, P. Q. Liao, J. Xu, G. Ouyang, J. P. Zhang and X. M. Chen, *J. Am. Chem. Soc.*, 2015, **137**, 7217–7223.

17 H. Amrouche, B. Creton, F. Siperstein and C. Nieto-Draghi, *RSC Adv.*, 2012, **2**, 6028.

18 A. U. Ortiz, A. P. Freitas, A. Boutin, A. H. Fuchs and F. X. Coudert, *Phys. Chem. Chem. Phys.*, 2014, **16**, 9940–9949.

19 K. Zhang, A. Nalaparaju, Y. Chen and J. Jiang, *Phys. Chem. Chem. Phys.*, 2014, **16**, 9643–9655.

20 K. Zhang, K. M. Gupta, Y. Chen and J. Jiang, *AIChE J.*, 2015, **61**, 2763–2775.

21 W. Morris, C. J. Doonan, H. Furukawa, R. Banerjee and O. M. Yaghi, *J. Am. Chem. Soc.*, 2008, **130**, 12626–12627.

22 W. Morris, B. Leung, H. Furukawa, O. K. Yaghi, N. He, H. Hayashi, H. Yao, M. Asta, B. B. Laird and O. M. Yaghi, *J. Am. Chem. Soc.*, 2010, **132**, 11006–11008.

23 M. Baias, A. Lesage, S. Aguado, J. Canivet, V. Moizan-Basle, N. Audebrand, D. Farrusseng and L. Emsley, *Angew. Chem.*, 2015, **54**, 5971–5976.

24 X.-C. Huang, Y.-Y. Lin, J.-P. Zhang and X.-M. Chen, *Angew. Chem.*, 2006, **118**, 1587–1589.

25 R. Banerjee, A. Phan, B. Wang, C. Knobler, H. Furukawa, M. O'Keeffe and O. M. Yaghi, *Science*, 2008, **319**, 939–943.

26 W. L. Jorgensen, J. Chandrasekhar, J. D. Madura, R. W. Impey and M. L. Klein, *J. Chem. Phys.*, 1983, **79**, 926–935.

27 P. Mark and L. Nilsson, *J. Phys. Chem. A*, 2001, **105**, 9954–9960.

28 L. Zhang, G. Wu and J. Jiang, *J. Phys. Chem. C*, 2014, **118**, 8788–8794.

29 Dassault Systèmes BIOVIA, *Materials Studio Modeling Environment, Release 2017*, Dassault Systèmes BIOVIA, San Diego, CA, 2016.

30 S. Aguado, J. Canivet and D. Farrusseng, *Chem. Commun.*, 2010, **46**, 7999–8001.

31 W. Morris, N. He, K. G. Ray, P. Klonowski, H. Furukawa, I. N. Daniels, Y. A. Houndonougbo, M. Asta, O. M. Yaghi and B. B. Laird, *J. Phys. Chem. C*, 2012, **116**, 24084–24090.